SRF CAVITY DETUNING CHARACTERIZATION BY CONTINUOUS WAVELET TRANSFORM: A TIME-FREQUENCY ANALYSIS*

J. S. Romero[2], P. Echevarria[1], J. Knobloch[1,3], A. Neumann[1], A. Ushakov[1], C. M. Cuesta[2]
[1]Helmholtz-Zentrum Berlin für Materialien und Energie, Berlin, Germany
[2]University of the Basque Country, Leioa, Spain
[3]University of Siegen, Siegen, Germany

Abstract

Sustainability is a key issue for both current and future particle accelerators. Superconducting RF (SRF) cavities with high loaded quality factors help reduce energy consumption in particle accelerators and the initial investment in RF amplifiers, but their narrow bandwidth makes them strongly susceptible to microphonic detuning.

To support the development of effective mitigation schemes, we apply the Continuous Wavelet Transform (CWT) to detuning signals measured at Helmholtz-Zentrum Berlin (HZB). While stationary microphonic components are already identified by conventional Fourier analysis, the CWT reveals sharp transient detuning bursts and impact-like activity, likely caused by mechanical or cryogenic disturbances. These results show that time-frequency analysis is essential for capturing the full microphonic environment.

INTRODUCTION

Particle accelerators are not immune to the current political, social, and economic situation. In this regard, both climate change and rising energy costs make sustainability a key consideration in both existing accelerators and future projects, [1]. Different research projects funded by the European Union [2, 3] are studying different strategies to tackle this issue. One of the tasks in Ref. [2] is to find ways to save energy from the RF power. More specifically in the case of low beam loading applications, as it is also stated in the European Roadmap for Particle Physics, [4], one major challenge due to the very small intrinsic cavity bandwidth is the sensitivity to small mechanical vibrations, commonly known as microphonics.

While active compensation via the cavity tuner is an open field of research, [5–10], passive measures like cryoplant operation optimization, vacuum pump isolation, etc., should always be considered in the first place, [11]. For these measures to be effective, a proper characterization of microphonics is fundamental.

The analysis of detuning signals requires tools capable of capturing time-dependent spectral variations. Classical Fourier analysis provides a global description that does not retain temporal information. To address this limitation, extensions such as the short-time Fourier transform (STFT) introduce time localization by applying the transform over sliding windows. However, the STFT uses a fixed window length, leading to a trade-off between time and frequency resolution that remains constant across all frequencies. This can be limiting for cavity detuning signals, where slow drifts and fast transient events may coexist.

For this reason, the CWT is used in this work as in Refs. [6, 12], as it provides a time-frequency representation with adaptive resolution [13]. The wavelet transform of a continuous time signal, $x(t)$, is defined as

$$T(a,b) = \frac{1}{\sqrt{a}} \int_{-\infty}^{\infty} x(t)\psi^* \left(\frac{t-b}{a}\right) \mathrm{d}t,$$

where $\psi(t)^*$ is the complex conjugate of the wavelet function $\psi(t)$, a is the scale parameter (inversely related to frequency), and b is the time-shift parameter of the wavelet. This formulation represents the signal as a superposition of time-localized contributions at different scales and positions. Different choices of wavelet function $\psi(t)$ emphasize specific signal features; for instance, commonly used wavelets such as Morlet or Mexican hat offer different compromises between time and frequency localization. For this work, the complex Morlet wavelet is used,

$$\psi(t) = \frac{1}{\sqrt{\pi B}} e^{2\pi i F t} e^{-t^2/B},$$

as it offers a well-defined central frequency and is particularly suitable for analyzing oscillatory signals. The specific parameters used are $F = 1.5$ and $B = 2.5$, where F is the center frequency and B is the bandwidth parameter. Scales a are logarithmically spaced from 1 to 1000, and the corresponding frequencies are derived from the sampling period using the PyWavelets library [14]. The scalogram amplitude is computed as the magnitude of the complex CWT coefficients, without any additional normalization; absolute

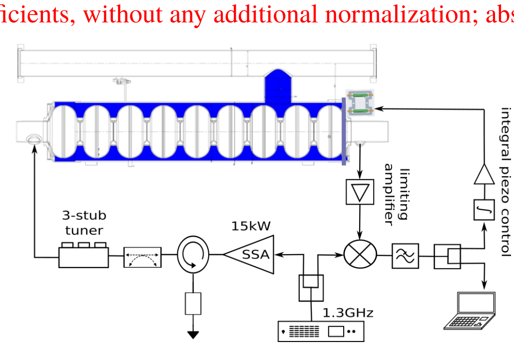

Figure 1: Experiment setup at HoBiCaT for detuning measurements.

* This project has received funding from the European Union's Horizon Europe research and innovation program under grant agreement N. 101131435 and from the Global Training Program, an initiative of Basque Trade and Investment, SPRI and Basque Government (Spain).

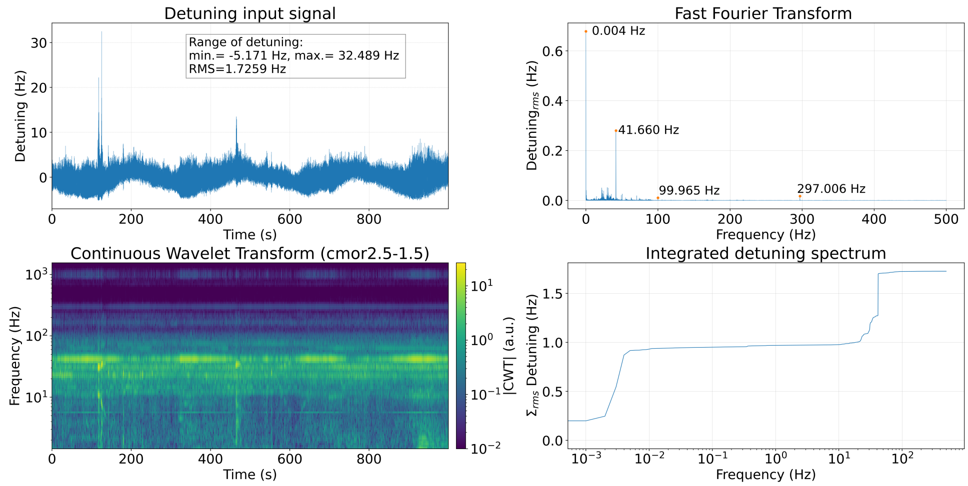

Figure 2: Detuning analysis at $Q_L = 4.5 \times 10^7$: raw detuning signal (top left), FFT spectrum (top right), CWT scalogram (bottom left), and integrated RMS detuning spectrum (bottom right).

values can therefore be compared within a given dataset, but not across datasets. Edge effects inherent to the finite signal length are not explicitly treated and features near the boundaries should be interpreted with caution.

EXPERIMENT SETUP AND RESULTS

The results shown in this paper were obtained in the HoBiCaT facility at HZB, [15,16], using a TESLA cavity, but also briefly during the first beam commissioning of SEALab's photoinjector, [17,18].

In order to measure the detuning of a cavity, we express it as

$$\Delta f(t) = \frac{f_0}{2Q_L} \tan(\Delta\Phi(t)),$$

where $\Delta f(t)$ is the detuning, f_0 the cavity's fundamental mode's frequency, Q_L the effective loaded quality factor and $\Delta\Phi(t)$ the phase difference between the forward and transmitted signals.

Figure 1 shows the measurement setup: a signal generator sends the 1.3 GHz signal to a 15 kW Solid State Amplifier (SSA) which is followed by a motorized three-stub tuner, located in the RF waveguide supply line outside the cryostat, to externally modify the Q_L. Then, the transmitted signal from the pickup antenna is leveled, amplified, and mixed with the forward signal. The result is low-pass filtered, acquired and stored for analysis. A slow piezoactuator integral control was also added to compensate for slow drifts, allowing longer time windows to be captured. Prior to its analysis, the DC component of the signal was removed by subtracting the mean value. No additional filtering or smoothing was applied. The integrated RMS detuning spectrum was then computed as $\Delta f_{\mathrm{rms}}(f_n) = \frac{\sqrt{\sum_{i=1}^{n} [F[\Delta f(t)]_i]^2}}{\sqrt{2}}$, where $F[\Delta f]_i$ is the Fourier component of index i.

Unfortunately, a technical problem with a getter pump caused a vacuum event in the cavity, after which the radiation onset field was around 5 MV/m. Detuning signals were acquired under continuous wave (CW) operation at two different loaded quality factors, $Q_L = 4.5 \times 10^7$ and $Q_L = 8.6 \times 10^6$, and over a time window of approximately 16 minutes each at a rate of 1000 samples per second. Figures 2 and 3 show the analysis for both Q_L values.

At $Q_L = 4.5 \times 10^7$ (Fig. 2), the cavity bandwidth narrows to approximately 29 Hz, making the detuning signal highly sensitive to any mechanical perturbation. The signal spans from −5.171 Hz to 32.489 Hz and exhibits two sharp transient detuning events at approximately $t = 120$ s and $t = 480$ s, which appear as short-lived broadband bursts in the time-frequency map. The FFT is dominated by a component near 0 Hz, reflecting slow non-stationary drifts whose timescale is comparable to the measurement window. A component at 41.660 Hz and weaker ones at 99.965 Hz and 297.006 Hz are also identified.

At $Q_L = 8.6 \times 10^6$ (Fig. 3), the wider cavity bandwidth of approximately 151 Hz results in a less sensitive detuning signal, with a range of ±10 Hz and no sharp transient events. As both measurements were acquired consecutively one hour apart, with only the Q_L adjusted via the three-stub tuner, the observed differences reflect the change in cavity sensitivity rather than a change in the mechanical environment. The reduced influence of slow drifts in this measurement is reflected in the FFT, where a richer microphonics spectrum becomes visible, with a dominant peak at 41.6 Hz and additional components at 100, 168.3, 217.7 and 297 Hz. The CWT confirms these as persistent narrowband features continuously present throughout the measurement. The integrated RMS spectrum shows a gradual accumulation of detuning contributions with clear steps at approximately 10 Hz and 40 Hz, reaching a total RMS detuning of approximately 1.9 Hz. The RMS remains comparable, as it is dominated by persistent rather than transient contributions.

The component at 297 Hz, present in both HoBiCaT measurements, is suspected to be the operating frequency of the helium pumping system at HoBiCaT. Meanwhile, the 41.6 Hz component present in both measurements is consistent with a known mechanical resonance mode of the cavity [6, 10].

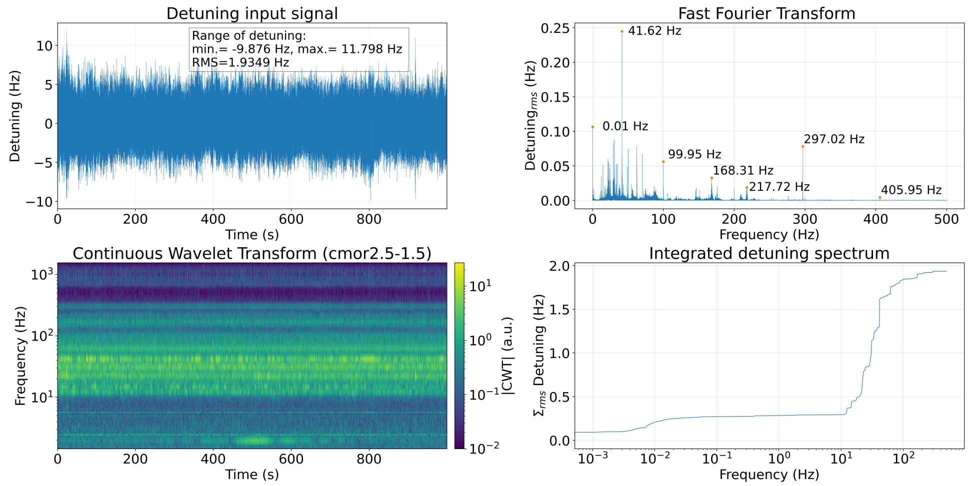

Figure 3: Detuning analysis at $Q_L = 8.6 \times 10^6$: raw detuning signal (top left), FFT spectrum (top right), CWT scalogram (bottom left), and integrated RMS detuning spectrum (bottom right).

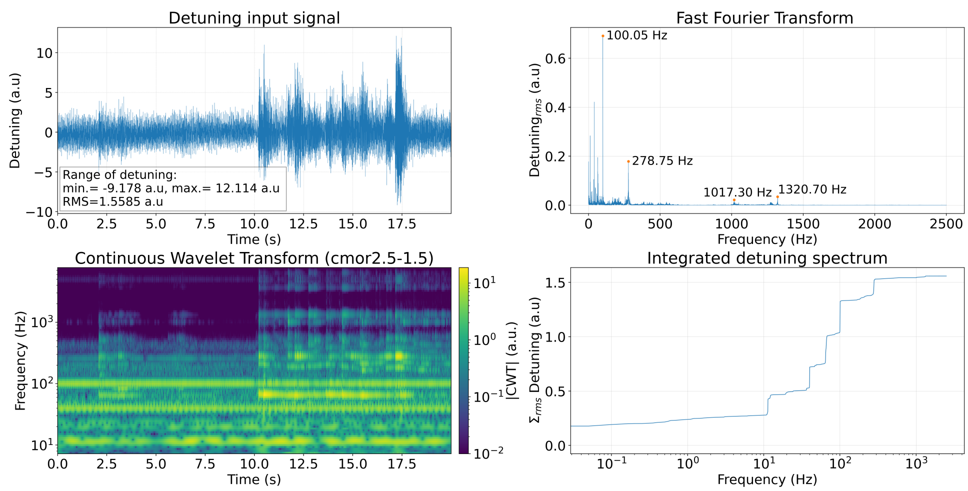

Figure 4: Detuning analysis of SEALab's photoinjector at $Q_L = 2.95 \times 10^7$: raw detuning signal (top left), FFT spectrum (top right), CWT scalogram (bottom left), and integrated RMS detuning spectrum (bottom right).

A similar setup to the one described above was also used during the first commissioning of SEALab's photoinjector, excluding the slow integral control. Figure 4 shows the corresponding analysis of the detuning signal recorded at a rate of 5000 samples per second, where impact-like detunings were observed; these appear in the CWT as localized bursts. While the FFT identifies dominant components at 100 Hz and 278.8 Hz, with weaker contributions at 1017.3 Hz and 1320.7 Hz, the CWT reveals that some components are not continuously present and only appear during the burst activity. A persistent low-frequency component near 10 Hz is also observed throughout the full measurement window. The integrated RMS spectrum confirms dominant contributions at ~10 Hz and 100 Hz, with an additional step at ~1000 Hz associated with the high-frequency transient content. It is suspected that these kinds of events are caused by the cryogenic system, and this case illustrates particularly well the capability of the CWT to resolve transient microphonic effects that would otherwise be masked in a spectral analysis.

CONCLUSIONS

In this work, the CWT has been applied to SRF cavity detuning signals measured in a TESLA cavity at HoBiCaT and in SEALab's photoinjector. The results demonstrate that the CWT provides a more complete characterization of microphonics than conventional Fourier-based approaches, particularly in the presence of transient and non-stationary detuning events. While the FFT identifies the frequency content of persistent components, it fails to capture the temporal evolution of transient bursts, which appear clearly as localized features in the CWT time-frequency maps. This was especially evident in the data collected at SEALab, where impact-like detuning events were shown to activate a 100 Hz component only during the burst activity.

Future work will focus on extending the analysis to longer datasets and different operating conditions. The use of accelerometers in combination with the CWT is also planned to correlate mechanical vibration sources with the observed detuning features, supporting the development of more effective microphonics mitigation strategies.

REFERENCES

[1] M. Benedikt *et al.*, "Future Circular Collider Feasibility Study Report", CERN, Geneva, Switzerland, Rep. 17, 2025. doi:10.17181/CERN.I26X.V4VF

[2] iSAS: Innovate for Sustainable Accelerating Systems, https://isas.ijclab.in2p3.fr/

[3] RF2.0 Research Facility: towards a more energy-efficient and sustainable path, https://rf20.eu/

[4] C. Adolphsen *et al.*, "European Strategy for Particle Physics - Accelerator R&D Roadmap", CERN, Geneva, Switzerland, Rep. CERN-2022-001, 2022. doi:10.23731/CYRM-2022-001

[5] Z. A. Conway and M. Liepe, "Fast Piezoelectric Actuator Control of Microphonics in the CW Cornell ERL Injector Cryomodule", in *Proc. PAC'09*, Vancouver, Canada, May 2009, paper TU5PFP043, pp. 918–920. https://jacow.org/PAC2009/papers/TU5PFP043.pdf

[6] A. Neumann, W. Anders, O. Kugeler, and J. Knobloch, "Analysis and active compensation of microphonics in continuous wave narrow-bandwidth superconducting cavities", *Phys. Rev. Spec. Top. Accel. Beams*, vol. 13, no. 8, p. 082001, Aug. 2010. doi:10.1103/PhysRevSTAB.13.082001

[7] J. P. Holzbauer *et al.*, "Active microphonics compensation for LCLS-II", in *Proc. IPAC'18*, Vancouver, Canada, Apr.-May 2018, pp. 2687–2689. doi:10.18429/JACoW-IPAC2018-WEPML007

[8] N. Banerjee, G. Hoffstaetter, M. Liepe, P. Quigley, and Z. Zhou, "Active suppression of microphonics detuning in high Q_L cavities", *Phys. Rev. Accel. Beams*, vol. 22, no. 5, p. 052002, May 2019. doi:10.1103/PhysRevAccelBeams.22.052002

[9] A. Bellandi, J. Branlard, H. Schlarb, and C. Schmidt, "Feedforward resonance control for the european x-ray free electron laser high duty cycle upgrade", *Front. Phys.*, vol. 11, 2023. doi:10.3389/fphy.2023.1170175

[10] A. Elejaga, J. Jugo, P. Echevarria, A. Neumann, A. Ushakov, and J. Knobloch, "Experimental testing of a modified active disturbance rejection control for microphonics reduction in a 9-cell tesla superconducting cavity", *Phys. Rev. Accel. Beams*, vol. 27, no. 11, p. 113501, Nov. 2024. doi:10.1103/PhysRevAccelBeams.27.113501

[11] J. P. Holzbauer *et al.*, "Passive microphonics mitigation during LCLS-II cryomodule testing at Fermilab", in *Proc. IPAC'18*, Vancouver, Canada, Apr.-May 2018, pp. 2668–2670. doi:10.18429/JACoW-IPAC2018-WEPML001

[12] F. Qiu *et al.*, "Analytical modeling and experimental verification of oscillatory ponderomotive instabilities in closed-loop superconducting rf cavities", *Phys. Rev. Accel. Beams*, vol. 28, no. 11, p. 112001, Nov. 2025. doi:10.1103/hs5q-q5xc

[13] S. Mallat, *A wavelet tour of signal processing*. San Diego: Academic Press, 1999. doi:10.1016/B978-012466606-1/50002-7

[14] G. R. Lee, R. Gommers, F. Waselewski, K. Wohlfahrt, and A. O'Leary, "Pywavelets: a python package for wavelet analysis", *Journal of Open Source Software*, vol. 4, no. 36, p. 1237, 2019. doi:10.21105/joss.01237

[15] J. Knobloch, W. Anders, D. Pflückhahn, and M. Schuster, "HoBiCaT - A test facility for superconducting RF systems", in *Proc. SRF'03*, Lübeck, Germany, Sep. 2003, paper MOP48, pp. 173–175. https://jacow.org/SRF2003/papers/MOP48.pdf

[16] O. Kugeler, A. Neumann, W. Anders, and J. Knobloch, "Adapting TESLA technology for future cw light sources using HoBiCaT", *Rev. Sci. Instrum.*, vol. 81, no. 7, p. 074701, Jul. 2010. doi:10.1063/1.3443561

[17] T. Kamps *et al.*, "Accelerator physics experiments at the versatile SRF photoinjector of SEALab", in *Proc. IPAC'23*, Venice, Italy, Sep. 2023, pp. 2115–2118. doi:10.18429/JACoW-IPAC2023-TUPL160

[18] T. Kamps *et al.*, "First beam commissioning of the HZB SRF photoelectron gun", in *Proc. IPAC'25*, Taipei, Taiwan, Nov. 2025, pp. 1718–1721. doi:10.18429/JACoW-IPAC2025-WECN2